

RESEARCH ARTICLE

Influence of layered skull modeling on the frequency sensitivity and target accuracy in simulations of transcranial current stimulation

Heng Wang¹  | Weiqian Sun² | Jianxu Zhang¹ | Zilong Yan¹ |
Chenyu Wang¹ | Luyao Wang¹ | Tiantian Liu² | Chunlin Li³  |
Duanduan Chen² | Funahashi Shintaro² | Jinglong Wu^{1,4} | Tianyi Yan² 

¹School of Mechatronics Engineering, Beijing Institute of Technology, Beijing, China

²School of Life Science, Beijing Institute of Technology, Beijing, China

³School of Biomedical Engineering, Capital Medical University, Beijing, China

⁴Department of Neurology and Neuroscience, Okayama University, Okayama, Japan

Correspondence

Tianyi Yan, School of Life Science, Beijing Institute of Technology, Beijing, China.
Email: yantianyi@bit.edu.cn

Funding information

the Beijing Municipal Science and Technology Commission, Grant/Award Number: Z191100010618004, Z201100007720009; the National Key R&D Program of China, Grant/Award Number: 2018YFC0115400; the National Natural Science Foundation of China, Grant/Award Numbers: U20A20191, 61727807, 82071912, 81771909

Abstract

With the development of electrical stimulation technology, especially the emergence of temporally interfering (TI) stimulation, it is necessary to discuss the influence of current frequency on stimulation intensity. Accurate skull modeling is important for transcranial current stimulation (tCS) simulation prediction because of its large role in dispersing current. In this study, we simulated different frequencies of transcranial alternating current stimulation (tACS) and TI stimulation in single-layer and layered skull model, compared the electric field via error parameters such as the relative difference measure and relative magnification factor. Pearson correlation analysis and *t*-test were used to measure the differences in envelope amplitude. The results showed that the intensity of electric field in the brain generated by per unit of stimulation current will increase with current frequency, and the layered skull model had a better response to frequency. An obvious pattern difference was found between the electric fields of the layered and single-layer skull individualized models. For TI stimulation, the Pearson correlation coefficient between the envelope distribution of the layered skull model and the single-layer skull was only 0.746 in the individualized model, which is clearly lower than the correlation coefficient of 0.999 determined from the spherical model. Higher carrier frequencies seemed to be easier to generate a large enough brain electric field envelope in TI stimulation. In conclusion, we recommend using layered skull models instead of single-layer skull models in tCS (particularly TI stimulation) simulation studies in order to improve the accuracy of the prediction of stimulus intensity and stimulus target.

KEYWORDS

electrical stimulation, individualized model, layered skull model, temporally interfering stimulation

1 | INTRODUCTION

Transcranial current stimulation (tCS) refers to a set of noninvasive neuromodulatory techniques that deliver weak electric currents to the brain through electrodes on the scalp (Nitsche et al., 2003; Schulz, Gerloff, & Hummel, 2013; Tavakoli & Yun, 2017). It includes transcranial direct current stimulation (tDCS), transcranial alternating current stimulation (tACS) and transcranial random noise stimulation (tRNS). Though similar in nature, these techniques have different physiological and behavioral effects (Ali, Sellers, & Frohlich, 2013; Daa, Atc, Gbasc, et al., 2019; Laakso, Mikkonen, Koyama, Hirata, & Tanaka, 2019) due to the different temporal profiles of the applied currents. In view of its safe and inexpensive features, tCS has been used for pain relief (O'Connell, Marston, Spencer, DeSouza, & Wand, 2018), depressive symptom relief (Mutz, Edgcumbe, Brunoni, & Fu, 2018), stroke (Fujimoto et al., 2016) and Parkinson's disease recovery (Elsner, Kugler, Pohl, & Mehrholz, 2016; Fregni et al., 2006; Kaski, Allum, Bronstein, & Dominguez, 2014; Kaski, Dominguez, Allum, Islam, & Bronstein, 2014), and in the treatment of epilepsy (Holmes et al., 2019). Over the last several years, new tCS approaches using multiple kHz currents have been proposed to stimulate deep targets (Grossman et al., 2017) or increase the intensity of stimulation (Voroslakos et al., 2018). Temporally interfering electrical stimulation recruits neural firing by envelope modulation of the electric field provided by multiple high-frequency alternating currents to directly reach deep brain regions without affecting shallow brain regions (Grossman et al., 2017).

In many clinical trials, electrical stimulation electrodes have been placed on the scalp, and the underlying brain region was considered to be effectively stimulated by the current. However, some simulation studies have questioned the accuracy of such a method (Bikson, Datta, Rahman, & Scaturro, 2010). Individualized human head models have been made based on magnetic resonance imaging (MRI) to predict electric fields under electrical stimulation (Rashed, Gomez-Tames, & Hirata, 2020), and the obvious influences of some factors, such as electrode parameters (Chen, Zou, Tang, Ke, & He, 2019; Mikkonen, Laakso, Tanaka, & Hirata, 2020) and cerebrospinal fluid, were proposed (Indahlastari et al., 2020). The skull, due to its low electrical conductivity, plays a large role in blocking and dispersing current during tCS (Nielsen et al., 2018). This shows that accurate skull modeling is an important part of electrical stimulation simulation. In actuality, the skull is a three-layer structure consisting of the outer compacta, spongiosa with high conductivity, and inner compacta. However, in most electrical stimulation simulation studies, the skull is modeled as an isotropic single-layer structure (Puonti, Saturnino, Madsen, & Thielscher, 2020; Suh, Lee, & Kim, 2012). After discussing the necessity of a three-layered skull model, Sumientra concluded that in a spherical head model, one-layer approximations perform well to some degree (Rampersad, Stegeman, & Oostendorp, 2013). In order to simulate the electric fields of tCS with kHz frequency current in an individualized head model containing an irregularly shaped spongy, the above conclusion will not be applicable because the spongy was modeled as a homogeneous spherical shell and the electrical stimulation was discussed only in the case of direct current.

In this study, we determined the effects of layered skull modeling on tCS simulation in a spherical head model and an individualized head model. To this end, we compared the results of tCS from two models, the ideal spherical model and the individualized head model, to determine the effect of the layered skull model. In addition, we wanted to study the effects of electrical stimulation frequency on electric field intensity because kHz tACS is used during temporally interfering electrical stimulation. We simulated tACS at different frequencies with a model in which the skull was separated into three layers and compared the electric field with the common isotropic single-layer skull model. The results showed that the layered skull model had a better response to the frequency, and a notable difference in the pattern was found between the electric field distributions of the layered skull and the single-layer skull individualized model. For temporally interfering electrical stimulation, the difference in the envelope amplitude was measured via Pearson correlation analysis and *t*-test. Finally, we considered that the carrier frequency has an effect on the stimulus intensity generated by unit currents. Therefore, we recommend using a layered skull model instead of an isotropic single-layer skull model in future tCS (particularly temporally interfering stimulation) simulation studies.

2 | MATERIALS AND METHODS

In order to study the influence of layered skull modeling on electrical stimulation, we constructed two kinds of models for finite element simulation: a spherical head model and an individualized human head model. Each kind of model can also be divided into a single-layer skull model and a layered skull model according to the degree of skull modeling refinement. We adopted the geometry of the spherical head model from the study by Rush and Driscoll (Rush & Driscoll, 1968) and applied the finite element method (FEM). Combined with CT and MRI data, we used the image segmentation method to reconstruct an individualized human head model and focused on refining the distribution of the compacta and spongiosa.

2.1 | Spherical head model

Three concentric spheres with radii of 77.5, 80, 85, and 92 mm constituted the single-layer skull spherical head model and represent the brain, cerebrospinal fluid (CSF), skull, and scalp, respectively (Datta, Elwassif, Battaglia, & Bikson, 2008; Rampersad et al., 2013). The electrodes were modeled as cylindrical patches with 10 mm radii and a thickness of 10 mm. Two such electrodes were placed on the outer sphere 90° apart, as shown in Figure 1a. The conductivities of the electrodes were chosen as 1.4 S/m for saline, and those for the brain, CSF and skin were chosen as 0.333, 1.5 and 0.435 S/m, respectively (Hauelsen, Ramon, Eiselt, Brauer, & Nowak, 1997). The bulk skull conductivity (σ_b) was 0.0042 S/m (Homma et al., 1995; Wolters et al., 2006). On the basis of the single-layer skull model, we subdivided the skull into the upper compacta, spongiosa, and lower

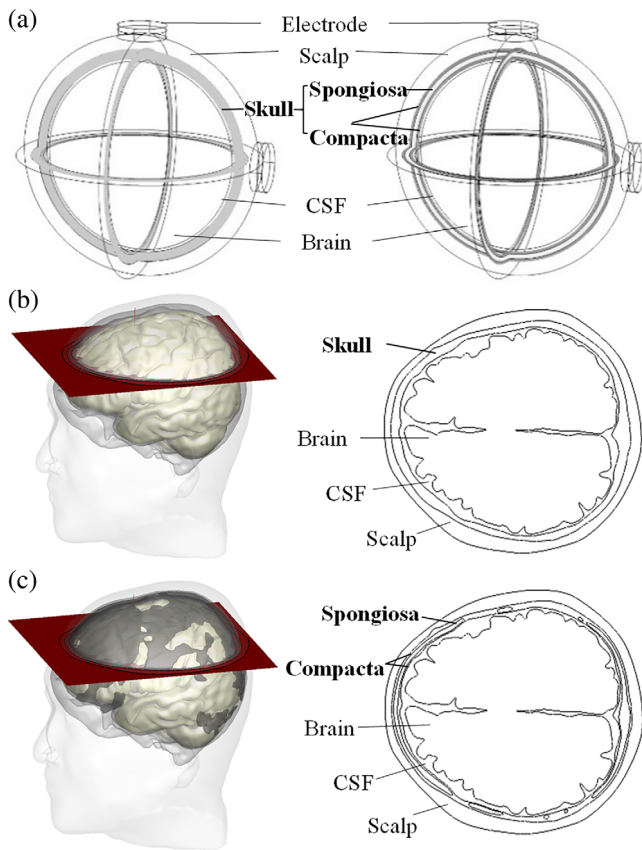


FIGURE 1 Schematic diagrams of the spherical head model and individualized head model. (a) Spherical head model; (b) Single-Layer skull individualized head model; (c) Layered skull individualized head model

compacta, thus modeling the layered skull model. According to the measurement results from existing studies (Akhtari et al., 2002), we divided the skull layers into 1.2, 2.3 and 1.5 mm layers, which represented the upper compacta, spongiosa, and lower compacta, respectively. There is a conversion relationship between the compacta conductivity (σ_c), spongiosa conductivity (σ_s) and bulk skull conductivity (σ_b) (Rampersad et al., 2013).

$$\frac{\sigma_c \sigma_s}{\lambda_c \sigma_s + \lambda_s \sigma_c} (\lambda_c \sigma_c + \lambda_s \sigma_s)^2 = \sigma_b^3 \quad (1)$$

$$\gamma = \frac{\sigma_s}{\sigma_c} \quad (2)$$

Here, λ_c is the ratio of the compacta thickness to the overall skull thickness; λ_s is the ratio of the spongiosa thickness to the overall skull thickness; and γ is the ratio between the conductivities of the compacta and spongy layers. According to the conductivity range of the compacta and spongiosa found in previous studies, the value of γ can vary from 1 to 20. We chose the middle three values $\gamma = 5$, $\gamma = 10$ and $\gamma = 15$ to construct the layered skull models. In addition, we set the relative permittivity (ϵ_r), to 10,000, 10,000, 110, and 3,000

for the skin, skull, CSF, and brain, respectively. The relative permittivities of compact and spongy materials are similar, and we set them uniformly at 10,000 (Gabriel, Gabriel, & Corthout, 1996).

$$\frac{1}{\sigma_r} = \frac{\lambda_c}{\sigma_c} + \frac{\lambda_s}{\sigma_s} \quad (3)$$

The single-layer skull model performed well in approximating the layered skull model when the skull compartment conductivity was equal to the equivalent radial conductivity (σ_r) of the layered skull model in tDCS (Rampersad et al., 2013). Therefore, the conductivity of the skull in the simulation of the single-layer skull model was chosen to be σ_r in our research.

2.2 | Individualized head model

We constructed a layered finite element model containing 2,274,767 grids, including the scalp, skull, CSF and brain, based on human MRI data. Two different head MR scans were collected with a 32-channel receive head coil on a 3 T GE scanner. Data covered the head and neck. The experimental protocol was approved by the Ethics Committee of Beijing Rehabilitation Hospital, Capital Medical University. The parameters were as follows: T1-weighted scan with fat suppression (T1fs): Spin-echo, 176 Sagittal slice, matrix size = 512×512 , voxel size = $0.58 \times 0.58 \times 1 \text{ mm}^3$, TR = 602 ms, TE = 14 ms, FA = 90° . T2-weighted scan (T2w): Spin-echo, 176 Sagittal slice, matrix size = 512×512 , voxel size = $0.58 \times 0.58 \times 1 \text{ mm}^3$, TR = 2,502 ms, TE = 85.724 ms, FA = 90° . SimNIBS was used for automatic segmentation of tissues including scalp, skull, CSF, and brain based on the complementary contrasts provided by the different sequences. The segmentation program mainly included the generation of mask for each tissue and morphological operations including opening, closing, and holes filling of the binary masks. Another open-source software, Meshfix, was used for repairing the head model, which can correct self-intersection and the intersection between different layers. The model needed to be checked before the simulation, and appropriate manual corrections were performed if necessary, mainly to delete some small channels or fill other holes.

In order to investigate the effects of layered skull modeling, two models were established. One type of skull had a single layer of uniform conductivity (Figure 1b), while the other was divided into three layers, representing the upper compacta, spongiosa, and lower compacta from outside to inside, respectively, as shown in Figure 1c. The general segmentation process did not automatically segment the spongiosa, so based on SimNIBS segmentation, the mask of spongiosa was extracted and reconstructed. Eroding one layer of voxel inward by the real skull mask. The eroded skull mask was multiplied with the T1fs image, and then the signal distribution of the skull area could be extracted. The geometry of the spongiosa was extracted based on the threshold of the histogram. Detailed operations:

1. Getting the real skull layer. The masks of the skull and CSF from SimNIBS were full of pixels internally. Subtracting the two can get the mask only representing the skull.
2. Eroding one layer of voxels inward from the real skull mask. Because of the inner and outer surfaces of the skull belonging to the compact bone, the erosion operation would not affect the correct modeling of the spongy bone.
3. Multiplying the eroded skull mask with the T1fs images. This operation can extract the signal distribution in the skull.
4. Reconstructing the spongy bone. The rough geometry of the spongy bone was extracted based on the threshold of the histogram, and manual correction was needed.
5. Meshing and optimizing by the open-source software, Gmsh.

The electrodes were modeled as cylindrical patches with 10 mm radii and a thickness of 10 mm. Two such electrodes were placed on the outer sphere 90° apart from the ideal model. The material of each layer was set to be uniform and isotropic, the conductivity and the relative permittivity (ϵ_r) were set to the same as those for the spherical head model.

2.3 | Computations

We studied two types of electrical stimulation: tACS and temporally interfering electrical stimulation. The distribution of electric field intensity in the brain needs to be estimated because it is an important indicator of the effect of tACS. The models were validated for grid independence. In order to simulate the process of electrical stimulation, current sources were applied on the electrodes at the scalp.

The Electric Conduction option calculates the current density (J) in conductors and lossy dielectrics. The basic governing equation for electric field finite element simulation is shown as equation $\frac{\partial \rho}{\partial t} + \nabla \cdot J = 0$, where J is the current density and ρ is the charge density. Substituting the Gaussian flux law and the isotropic constitutive equation $\nabla \cdot D = \rho$, $D = \epsilon E$ where D is the electrical displacement density, E is the electric field strength, and σ is the electrical conductivity, Equations (4) and (5) are accessible. Substituting $E = -\nabla \phi$ to rewrite the equation for the electric field solves (6).

$$\nabla \cdot \left[J + \frac{\partial D}{\partial t} \right] = 0 \quad (4)$$

$$\nabla \cdot \left[\sigma E + \frac{\partial \epsilon E}{\partial t} \right] = 0 \quad (5)$$

$$\nabla \cdot \left[\sigma \nabla \phi + \epsilon \frac{\sigma \nabla \phi}{\partial t} \right] = 0 \quad (6)$$

Electrical stimulation is a sinusoidal waveform, where the potential ϕ is converted into a complex form, and the electrical conduction equation is transformed into the frequency domain calculation equation $\nabla \cdot [\sigma + j\omega\epsilon] \nabla \phi = 0$, and a continuous time series of potentials under sinusoidal stimulation is obtained. This problem is transformed

into the solution of equation $\nabla \cdot \sigma \nabla \phi_i + \nabla \cdot \omega \epsilon \nabla \phi_j = 0$, and $\nabla \cdot \sigma \nabla \phi_j - \nabla \cdot \omega \epsilon \nabla \phi_i = 0$. The instantaneous electric field should then be solved by (7).

$$\nabla \cdot \left[\sigma \nabla \phi + \epsilon \nabla \frac{\partial \phi}{\partial t} \right] = 0 \quad (7)$$

For temporally interfering electrical stimulation, we estimated the distribution of the electric field envelope amplitude in the brain as the evaluation index of effectiveness. The first step in this process was to simulate the electric field intensity according to the above calculation method. Then, the obtained electric field strength can be calculated by (8) to obtain the electric field envelope amplitude.

$$|E_{AM}(\mathbf{n}, \mathbf{r})| = \left| |(\mathbf{E}_1(\mathbf{r}) + \mathbf{E}_2(\mathbf{r})) \cdot \mathbf{n}| - |(\mathbf{E}_1(\mathbf{r}) - \mathbf{E}_2(\mathbf{r})) \cdot \mathbf{n}| \right| \quad (8)$$

Here, \mathbf{E}_1 and \mathbf{E}_2 represent the fields generated by the first and second electrode pairs, respectively, \mathbf{n} is a unit vector along the direction that is studied, and \mathbf{r} represents the location. Then, we can draw the simulated distribution of the envelope amplitude of the electric field intensity.

2.4 | Analysis of tACS

With the development of electrical stimulation technology, the stimulation frequency span is no longer limited to less than 100 Hz. Since the real modulating effect of temporally interfering electrical stimulation on neurons is the modulating wave of two different kHz tACS, it is necessary to perform the simulation of kHz frequency tACS.

In order to explore the influence of stimulation frequency on the intensity and distribution of electrical stimulation, we stimulated the layered skull models ($\gamma = 5, 10, \text{ and } 15$) and the corresponding single-layer models on the electrodes on the scalp with the same current density $J = \sin(2\pi ft)$ uA/mm², where f is the frequency of tACS from 0 Hz to 1 kHz with a frequency interval of 100 Hz. The influence of γ values on the simulation results can also be analyzed. We mainly analyzed the electric field distribution in the regions representing the brain and recorded the maximum electric field intensity achieved in the brain of each model. Regarding the error of the distribution of electric field intensity between the single-layer skull model and the layered skull model, we used the relative magnification factor (MAG) and the relative difference measure (RDM).

$$RDM = \sqrt{\sum_{k=1}^m \left(\frac{\hat{E}_k}{\bar{E}} - \frac{E_k}{\bar{E}} \right)^2} \quad (9)$$

$$MAG = \left| 1 - \sqrt{\frac{\bar{E}}{\hat{E}}} \right| \quad (10)$$

Here, E_k is the electric field of each element in the single-layer skull model and \hat{E}_k is the electric field of each element in the layered

skull model. E is the norm of the electric field for all brain elements in the single-layer skull model and \hat{E} is that in the layered skull model.

2.5 | Analysis of temporally interfering electrical stimulation

We chose the layered skull model ($\gamma = 10$) and the corresponding single-layer skull model for the temporally interfering electrical stimulation simulation. A current density of $J_1 = \sin(2\pi f_1 t)$ uA/mm² was applied on the left two electrodes, and $J_2 = \sin(2\pi f_2 t)$ uA/mm² was applied on the right two electrodes ($f_1 = 1,000$ Hz, $f_2 = 1,010$ Hz). For temporally interfering electrical stimulation, the distribution of the electric field envelope changed according to the chosen field directions. We selected the X, Y, and Z directions to compare the envelope value distribution between the layered skull model and the single-layer skull model. Scatter diagrams were plotted, and Pearson correlation coefficients were calculated for the electric field envelope amplitude values of all elements in the two models. In addition, box plots were constructed, and t-test was performed to analyze the difference between the distribution electric field envelope of the single-layer skull model and the layered skull model.

In temporally interfering electrical stimulation, the electric field envelope drives neural spiking activity. Temporally interfering electrical stimulation at different carrier frequencies and fixed difference frequencies resulted in similar spike frequencies (Grossman et al., 2017). We used $\Delta f = 10$ Hz as the neuromodulation frequency and simulated TI stimulation under different carrier frequencies to determine the influence of carrier frequency. The envelope frequency was kept at 10 Hz, and the envelope field distributions of 500 Hz/510 Hz, 1,000 Hz/1010 Hz, and 1,500 Hz/1510 Hz were compared to discuss the influence of different carrier frequencies on the temporally interfering electrical stimulation.

3 | RESULTS

3.1 | tACS in the spherical head model.

Since transcranial electrical stimulation is used to stimulate the brain for the purpose of regulating brain function, we show the distribution of electric field intensity in the innermost layer representing the brain. In the layered skull model, we set the ratio of spongiosa and compacta conductivity to $\gamma = 5$, $\gamma = 10$, and $\gamma = 15$ and chose the skull conductivity σ_r in the corresponding single-layer skull model according to the simplified method. Each model was simulated with 0 Hz and 1 kHz tACS with a uniform colorbar. Figure 2ai shows the distribution of electric field intensity in the layered skull model ($\gamma = 5$) at 0 Hz tACS, and Figure 2aii displays that of 1 kHz tACS. The field intensity values of all elements were extracted in the same sequence, and Figure 2aiii shows the histogram of the difference between the two models. By comparing Figure 2ai and Figure 2aii, we found that 0 Hz tACS and

1 kHz tACS displayed differences in the layered skull model, and the tACS intensity of 1 kHz was higher than that of 0 Hz tACS. The histogram in Figure 2aiii also shows the difference between the electric field intensity between 1 kHz tACS and 0 Hz tACS. Figure 2b and Figure 2c show similar results, corresponding to the model $\gamma = 10$ and the model $\gamma = 15$, respectively. With increasing γ value, the field intensity of electric stimulation at 1 kHz tACS increased more clearly than that at 0 Hz. That is, the higher the ratio of spongiosa conductivity to compacta spongiosa, the more obvious the variation of simulated electric field intensity with frequency in the layered skull model.

We calculated the electric field intensities of the representative layers of the brain in each ideal sphere model at different frequencies of electrical stimulation. Figure 3a shows the relative maximum electric field intensities in the single-layer skull model and the layered skull model ($\gamma = 5$). The electric field intensities of all models tended to increase with increasing stimulus frequency. The red polyline representing the layered skull model has a higher slope than that of the yellow polyline representing the single-layer skull model, indicating that the stratification of the skull will increase the response of the model to the stimulation frequency during the simulation. Figure 3b and Figure 3c correspond to the $\gamma = 10$ and $\gamma = 15$ model results, respectively. When γ was 15, the electric field intensity of 1 kHz tACS was 1.2 times that at 0 Hz tACS in the layered skull model. Moreover, the larger the value of γ is, the more sensitive the model is to changes in stimulation frequency in the layered skull model.

Figure 4 displays the average electric field intensity errors in the brain compartment between the layered model and the single-layer model. As shown in Figure 4a, the error in MAG varies with frequency, and the models with a larger γ value have a larger fluctuation range. Figure 4b shows that the error in RDM decreases with increasing frequency, but the fluctuation range is very small (below 0.03) in the spherical head models. This indicates that the stratification of the skull in the ideal sphere model will not significantly affect the pattern of the electric field, but it will affect the overall intensity of the electric field.

3.2 | tACS in the individualized head model

Similar to the spherical head models, we performed the same simulation on the individualized human head models. In the layered skull model, we set the ratio of spongiosa and compacta conductivity to $\gamma = 5$, $\gamma = 10$, and $\gamma = 15$ and chose the skull conductivity as σ_r in the corresponding single-layer skull model to be exactly the same as that in the sphere model. Each model was simulated with 0 Hz and 1 kHz tACS with a uniform colorbar. Figure 5ai shows the distribution of the electric field intensity in the layered skull model ($\gamma = 5$) at 0 Hz tACS, and Figure 5aii displays that of 1 kHz tACS. The field intensity values of all elements were extracted in the same sequence, and Figure 5aiii shows the histogram of the difference between the two models. By comparing Figure 5ai and aii, we found that 0 Hz tACS and 1 kHz tACS displayed some differences in the layered skull model, and the tACS intensity of 1 kHz was higher than that of 0 Hz tACS. The histogram in Figure 5aiii also shows the difference between the electric

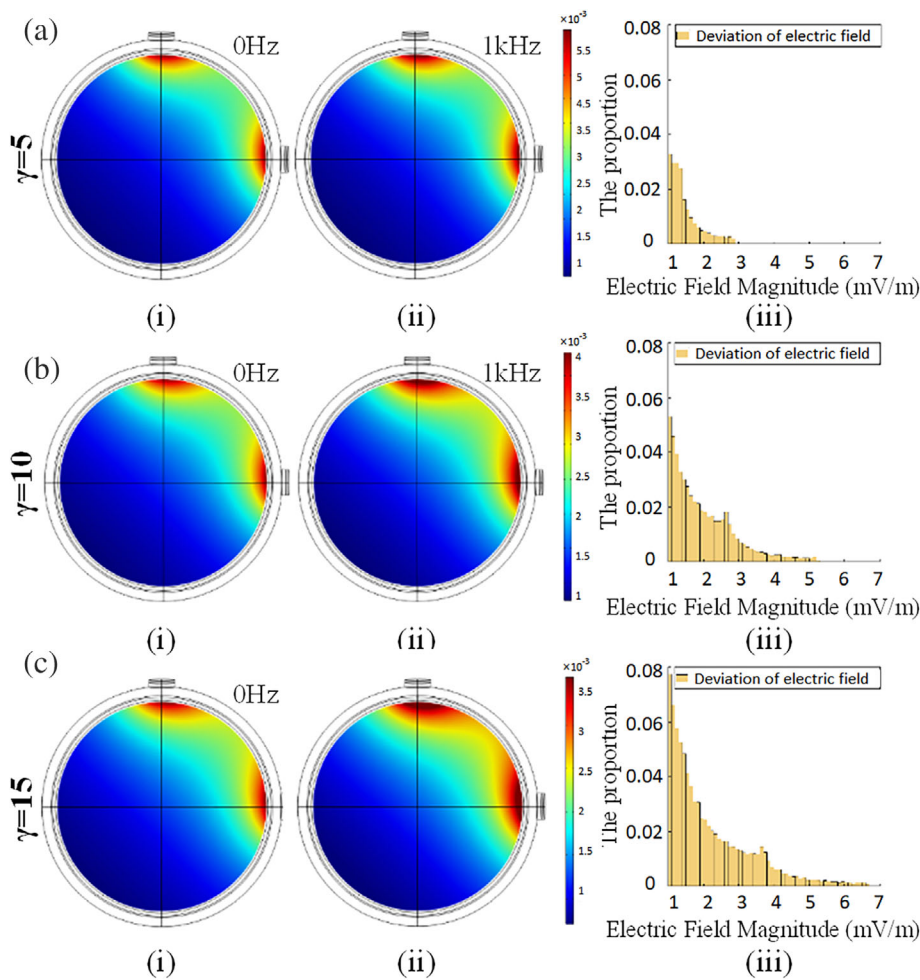


FIGURE 2 The electric field distribution of the spherical head models with a layered skull in 0 Hz and 1 kHz tACS. (a) i The electric field distribution, 0 Hz, $\gamma = 5$; (a) ii Electric field distribution, 1 kHz, $\gamma = 5$; (a) iii Histogram of the difference in electric field intensity between 0 Hz and 1 kHz, $\gamma = 5$. (b) i The electric field distribution, 0 Hz, $\gamma = 10$; (b) ii Electric field distribution, 1 kHz, $\gamma = 10$; (b) iii Histogram of the difference in electric field intensity between 0 Hz and 1 kHz, $\gamma = 10$. (c) i The electric field distribution, 0 Hz, $\gamma = 15$; (c) ii Electric field distribution, 1 kHz, $\gamma = 15$; (c) iii Histogram of the difference in electric field intensity between 0 Hz and 1 kHz, $\gamma = 15$

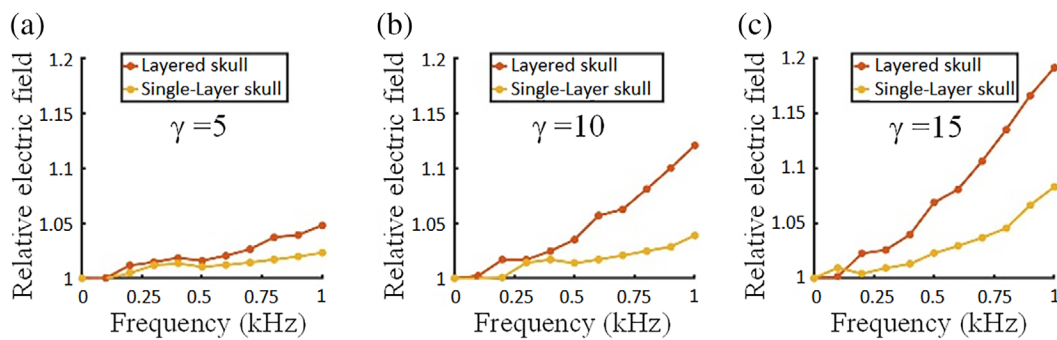


FIGURE 3 The relative electric field intensities in the spherical head models with a layered skull and a single-layer skull in tACS varies with frequency. (a) $\gamma = 5$; (b) $\gamma = 10$; (c) $\gamma = 15$

field intensity in 1 kHz tACS and that in 0 Hz tACS. Figure 5b and Figure 5c show similar results, corresponding to the $\gamma = 10$ and $\gamma = 15$ models. With an increase in the γ value, the field intensity of electric stimulation at 1 kHz tACS increases more obviously than that at 0 Hz. That is, the higher the ratio of spongiosa conductivity and compacta, the more obvious the variation of the simulated electric field intensity with frequency in the layered skull model. The results were the same for the individualized models and the ideal models.

We calculated the electric field intensity of the representative layers of the brain in each individualized head model at different frequencies of electrical stimulation. Figure 6a shows the relative maximum electric field intensity in the single-layer skull model and the layered skull model ($\gamma = 5$). The electric field intensity of all models tended to increase with increasing stimulus frequency. The red polyline representing the layered skull model had a higher slope than the yellow polyline representing the single-layer skull model,

indicating that the stratification of the skull will increase the response of the model to the stimulation frequency during the simulation. Figure 6b and Figure 6c correspond to the $\gamma = 10$ and $\gamma = 15$ model

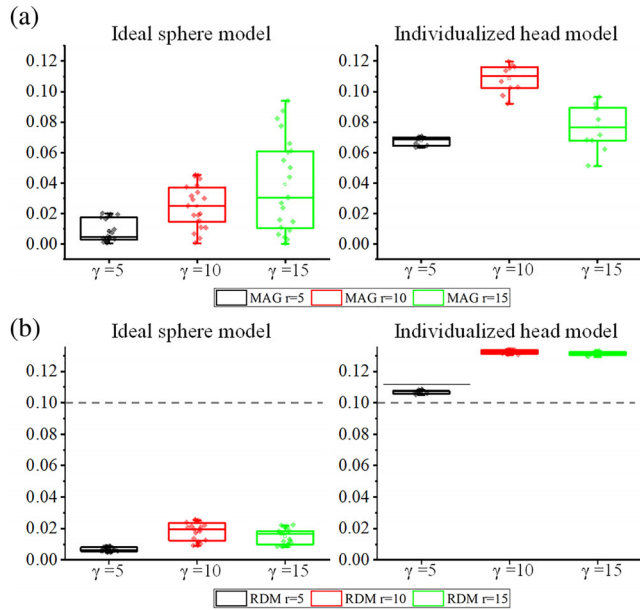


FIGURE 4 The average electric field intensity errors between the layered skull model and the corresponding single-layer skull model. (a) MAG in the ideal sphere models and MAG in the individualized head models. (b) RDM in the ideal sphere models and RDM in the individualized head models

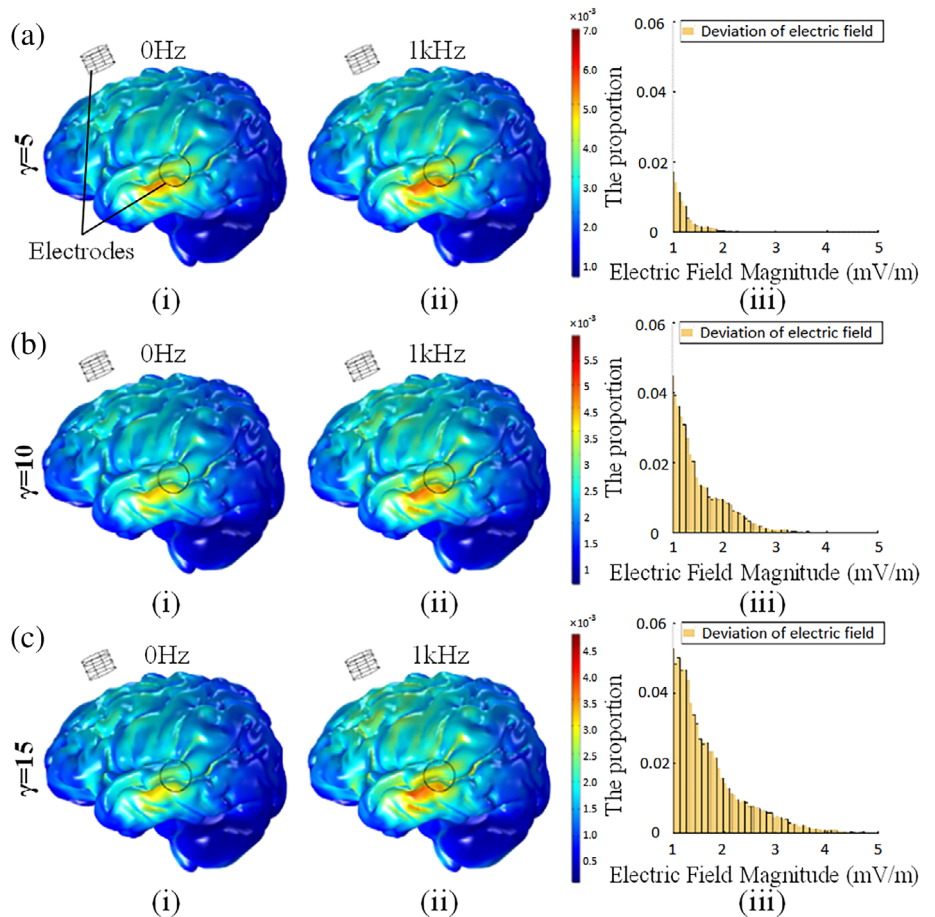
results, respectively. When γ was 15, the electric field intensity of 1 kHz tACS was 1.16 times that of 0 Hz tACS in the layered skull model. Moreover, the larger the value of γ is, the more sensitive the model is to the change in stimulation frequency in the layered skull model.

As shown in Figure 4a, the error in MAG varies with frequency, and the individualized head model with a larger γ value has a larger fluctuation range. Figure 4b shows that the RDM error decreases with increasing frequency in the individualized head models, but the fluctuation range is very small. Compared with the result of the spherical models, the RDM error of the individual models is larger as a whole (greater than 0.1). This indicates that the stratification of the skull in the individualized human head model will significantly affect the pattern of the electric field. However, stratification of the skull will affect the overall intensity of the electric field but not significantly affect the pattern of the electric field in ideal sphere models, which is the difference between the spherical models and the individualized models.

3.3 | Temporally interfering electrical stimulation

We previously discussed the frequency characteristics and differences between the layered skull and single-layer skull models in alternating current stimulation. Then, we discussed whether there is a difference in the electric field envelope distribution between the layered skull model and single-layer skull model in temporally interfering electrical stimulation. Figure 7a–c show the results of the ideal sphere model.

FIGURE 5 Effects of the ratio of compacta and spongiosa conductivity on the intensity of electrical stimulation in the brain. Electric field distribution of individualized head models with layered skulls in 0 Hz and 1 kHz tACS. (a) i The electric field distribution, 0 Hz, $\gamma = 5$; (a) ii Electric field distribution, 1 kHz, $\gamma = 5$; (a) iii Histogram of the difference in electric field intensity between 0 Hz and 1 kHz, $\gamma = 5$. (b) i The electric field distribution, 0 Hz, $\gamma = 10$; (b) ii electric field distribution, 1 kHz, $\gamma = 10$; (b) iii Histogram of the difference in electric field intensity between 0 Hz and 1 kHz, $\gamma = 10$. (c) i The electric field distribution, 0 Hz, $\gamma = 15$; (c) ii Electric field distribution, 1 kHz, $\gamma = 15$; (c) iii Histogram of the difference in electric field intensity between 0 Hz and 1 kHz, $\gamma = 15$



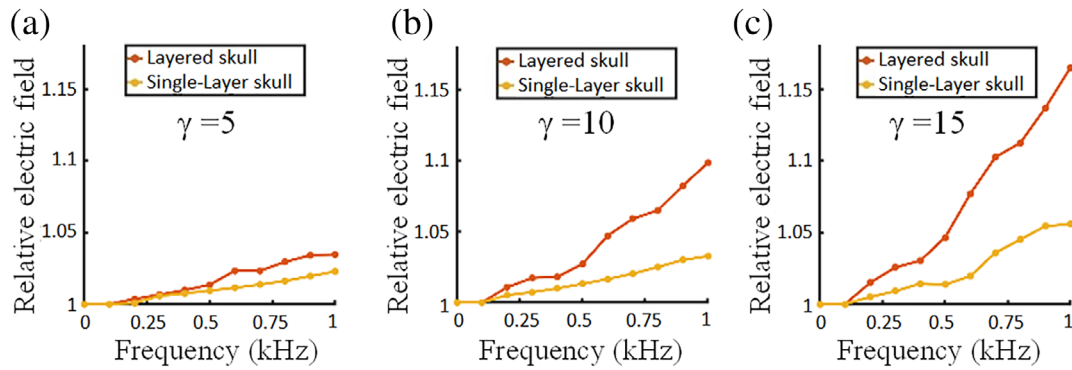


FIGURE 6 The maximum relative electric field intensity in the individualized head models with layered skull and single-layer skull in tACS varies with frequency: (a) $\gamma = 5$; (b) $\gamma = 10$; (c) $\gamma = 15$

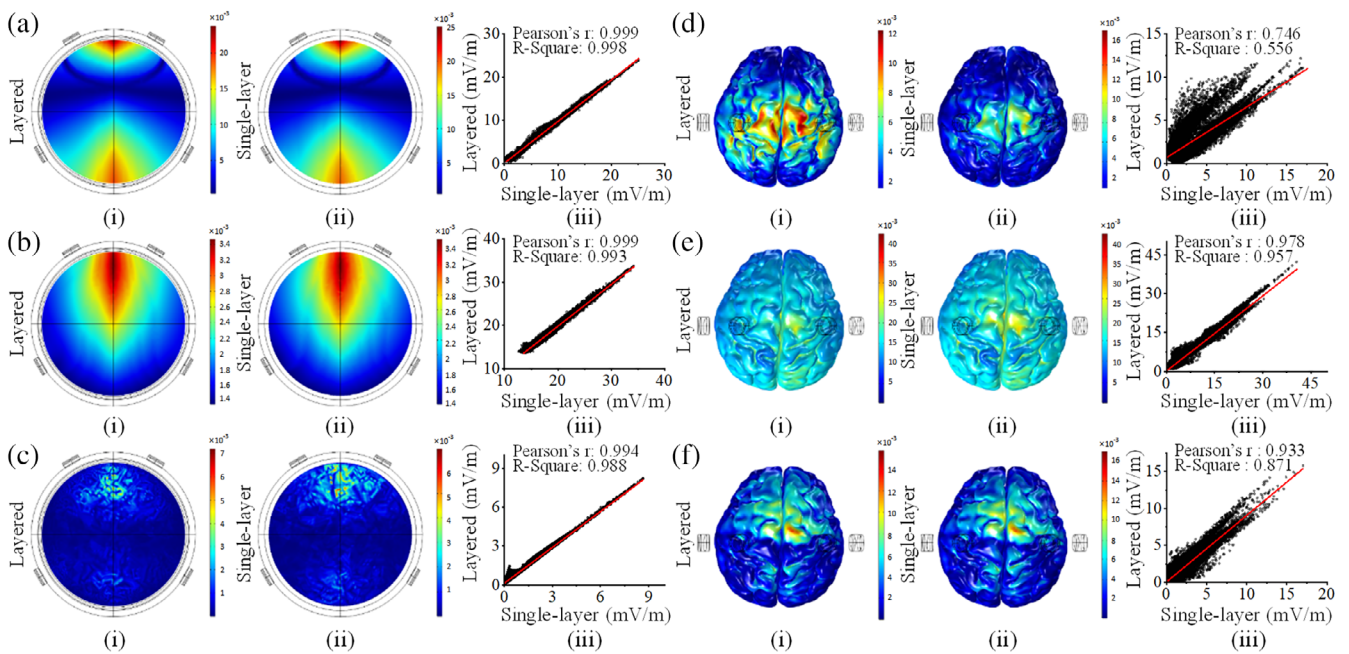


FIGURE 7 Distribution of the electric field envelope in the ideal sphere and individualized head models. (a) i Single-layer skull, ideal sphere, x-direction. ii Layered skull, ideal sphere, x-direction. iii Pearson correlation analysis, ideal sphere, x-direction. (b) i Single-layer skull, ideal sphere, x-direction. ii Layered skull, ideal sphere, x-direction. Iii Pearson correlation analysis, ideal sphere, x-direction. (c) i Single-layer skull, ideal sphere, x-direction. ii Layered skull, ideal sphere, x-direction. Iii Pearson correlation analysis, ideal sphere, x-direction. (d) i Single-layer skull, individualized head, x-direction. ii Layered skull, individualized head, x-direction. Iii Pearson correlation analysis, individualized head, x-direction. (e) i Single-layer skull, individualized head, x-direction. ii Layered skull, individualized head, x-direction. Iii Pearson correlation analysis, individualized head, x-direction. (f) i Single-layer skull, individualized head, x-direction. ii Layered skull, individualized head, x-direction. Iii Pearson correlation analysis, individualized head, x-direction

Figure 7ai shows the distribution of the electric field envelope in the single-layer skull model in the x-direction, and Figure 7aai shows the distribution of the electric field envelope in the layered skull model in the x-direction. By comparing Figure 7ai with Figure 7aai, it can be concluded that in the ideal sphere model, the layered skull has little influence on the distribution of the electric field envelope in the x-direction. Figure 7aaii shows the results of the Pearson correlation analysis between the electric field envelope values of the single-layer skull model and layered skull model in the x-direction, and the high

Pearson correlation coefficient of 0.999 reflects the high similarity of the two models. Similarly, Figure 7b and Figure 7c show the results of the electric field envelope in the y-direction and z-direction. Overall, the distributions of the electric field envelope in the three directions of the single-layer skull model and the layered skull model are very similar in the ideal sphere model via intuitive graph observation and correlation analysis. Figure 7d–f display the of the individualized head model results. Figure 7di shows the distribution of the electric field envelope in the single-layer skull model in the x-direction, and

Figure 7dii shows that of the layered skull model. By comparing Figure 7di with Figure 7dii, it can be concluded that the distribution of the *x*-direction electric field envelope amplitude is quite different between the single-layer skull model and the layered skull model in the individualized head models. Figure 7diii shows the Pearson correlation analysis results between the electric field envelope values of the single-layer skull model and the layered skull model in the *x*-direction, and the Pearson correlation coefficient of 0.746 was obviously smaller than that of the ideal sphere model shown in Figure 7aiii. Figure 7e and Figure 7f show the results of the electric field envelope in the *y*-direction and *z*-direction. There are some differences between the distributions of the electric field envelope in the *y*-directions of the single-layer skull model and the layered skull model by visual observation, as shown in Figure 7ei and eii. However, the Pearson correlation coefficient between the two models is relatively high, as shown in Figure 7eiii. The distributions of the *z*-direction electric field envelope of the single-layer skull model and the layered skull model were very similar, as shown in Figure 7fi and fii. However, the Pearson correlation coefficient between the two models was 0.933, as shown in Figure 7fiii.

In order to analyze the difference between the distribution electric field envelope of the single-layer skull model and the layered skull model from another perspective, we extracted the electric field envelope amplitude data from elements in the regions representing the brain. The data representing the envelope in the same direction of the single-layer skull model and layered skull model were drawn into a box plot, and a *t*-test was performed. Figure 8a shows the box plot of the electric field envelope amplitudes in the *x*, *y*, and *z* directions of the ideal sphere model with both a single-layer skull and layered skull. The *t*-test results show that there is no significant difference in the envelope amplitude distribution between the single-layer and layered skull ideal sphere models in the *x* and *z* directions. Figure 8b shows a bar diagram of the electric field envelope amplitudes in the *x*, *y*, and *z* directions of the individual head models with a single-layer skull and layered skull. The *t*-test results show that there are significant differences in the envelope amplitude

distribution of single-layer skull and layered skull individual head models in the *x*, *y*, and *z* directions. The results show that compared with the spherical head models, the difference in envelope amplitude between the layered and single-layer skull individual head models is more obvious.

Finally, we discuss the influence of carrier frequency in temporally interfering electrical stimulation. Figure 9 shows the distributions of the electric field envelope with different carrier frequencies and the Pearson correlation coefficients between them. In the spherical head model, with increasing carrier frequency, the envelope amplitude generated by the same current density stimulus increases, as shown in Figure 9a. The *x*-direction electric field envelope resulting from the 2 kHz carrier frequency is 1.35 times greater than that resulting from the 500 Hz carrier frequency. Notably, the Pearson correlation coefficient *r* between the simulation results of the different carrier frequencies is very high, which shows that the carrier frequency has little effect on the pattern of the electric field envelope amplitude. The results of the individualized head model are similar to the spherical head model. The *x*-direction electric field envelope resulting from the 2 kHz carrier frequency is 1.34 times greater than that resulting from the 500 Hz carrier frequency. The Pearson correlation coefficient *r* from these data is also high. Similar results are found in the other two directions as shown in Figure 9bc.

4 | DISCUSSION

Some research has concluded that isotropic single-layer skull approximations perform well to simulate the skull realistically with a spherical head model, and it is not necessary to model the three layers of skull separately (Rampersad et al., 2013). However, the spongy is not uniformly thick and distributed throughout the whole skull in the individualized model. Thus, the single-layer skull individualized head model may have some limitations in the simulation of tACS and temporally interfering electrical stimulation compared to the layered skull model. The proposition and development of temporally interfering electrical stimulation promoted the application of kHz tACS, so it became necessary to study whether the electric field intensity was different under different electrical stimulation frequencies.

In this study, we constructed ideal sphere models and individualized human head models and then performed finite element analysis of the electric field at different frequencies of tACS. We found that the electric field intensity in the brain increased with increasing stimulation frequency under the same current intensity which was consistent with the experimental result (Wang et al., 2020). By comparing the simulation results, we found that the electric field intensity of the layered skull model more obviously changed with the stimulation frequency than that of the single-layer skull model. The difference between the frequency-electric field intensity curves of the layered skull models and the single-layer skull models was greater when the ratio of spongy conductivity and compacta conductivity was greater. This phenomenon exists in both the ideal sphere models and

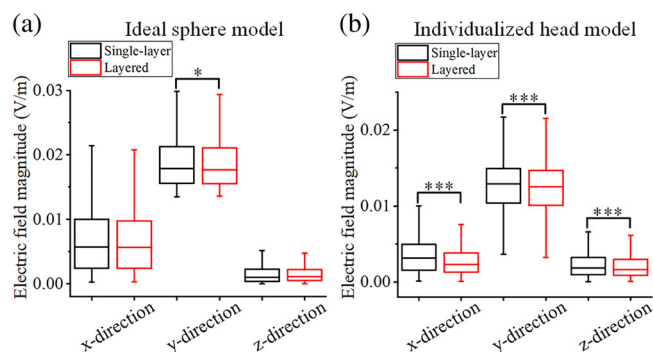


FIGURE 8 The bar diagrams and *t*-test results of the electric field envelope in the ideal sphere and individualized head model. (a) Ideal sphere model; (b) Individualized head model

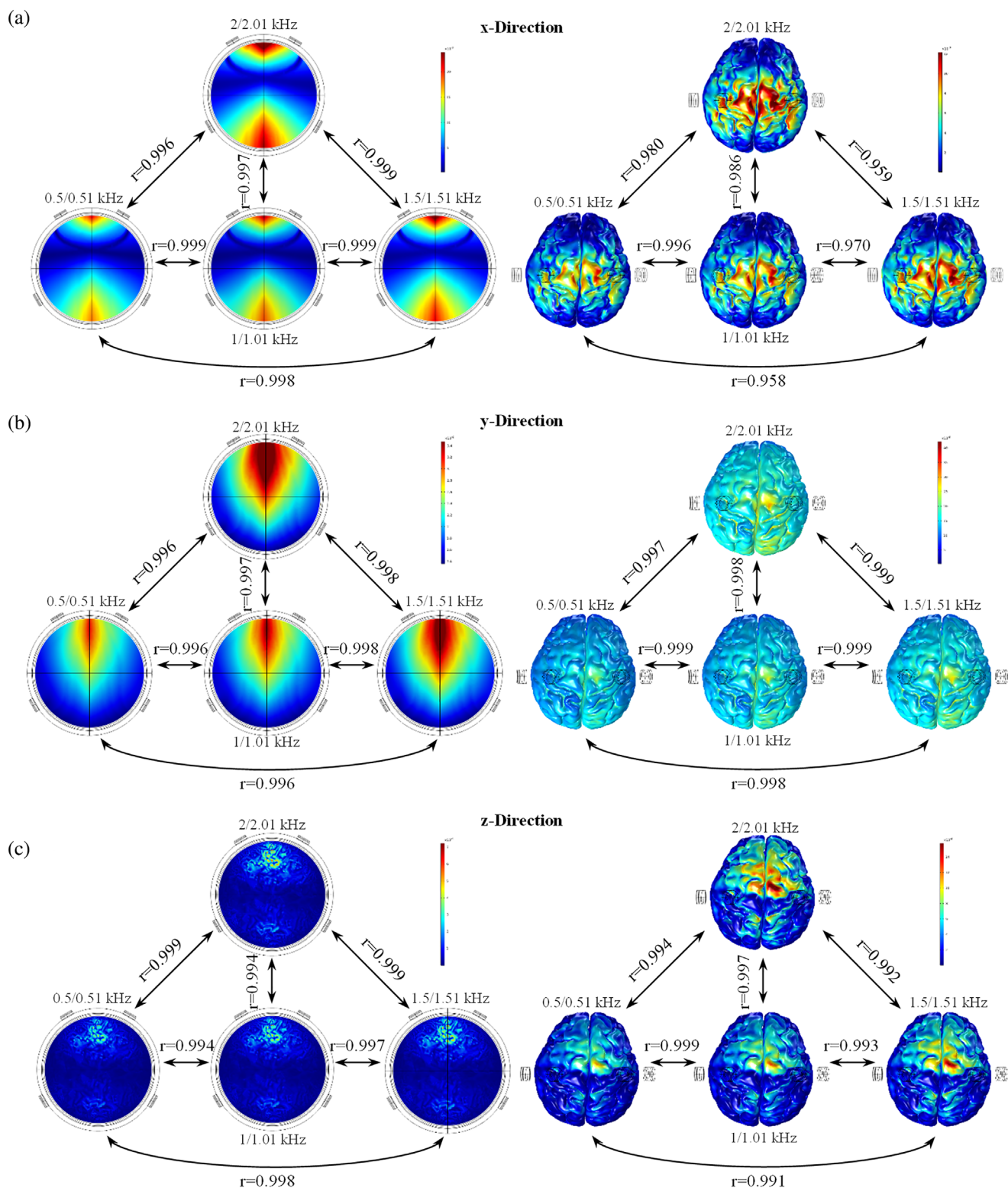


FIGURE 9 The distributions of the electric field envelope with different carrier frequencies and Pearson correlation coefficients between them. (a) The spherical head models and the individual head models: 0.5/0.51 kHz, 1/1.01 kHz, 1.5 kHz/1.51 kHz, 2/2.01 kHz in the x-direction. (b) The spherical head models and the individual head models: 0.5/0.51 kHz, 1/1.01 kHz, 1.5 kHz/1.51 kHz, 2/2.01 kHz in the y-direction. (c) The spherical head models and the individual head models: 0.5/0.51 kHz, 1/1.01 kHz, 1.5 kHz/1.51 kHz, 2/2.01 kHz in the z-direction

individual head models. According to the characteristics of electromagnetic conduction, small conductivity and large relative permittivity can make the electric field intensity of the model change obviously

with the frequency current. In the construction of the head model, differentiating the spongy and compacta caused the electrical conductivity of the portion of the skull to be much lower than that of the one-

layer skull. Therefore, the layered skull model would have better sensitivity to current frequency with the same relative permittivity.

With respect to the error of distribution of the electric field intensity between the single-layer skull model and the layered skull model, we found that within a certain frequency range, the larger the ratio between the conductivities of the compact and spongy layers was, the larger the MAG fluctuation range was. The other error, RDM, is generally lower than 0.025 in the ideal sphere models. However, in the individualized head models, the RDM error is generally larger than 0.1. MAG is a measure of the size of the errors and RDM is a measure of the pattern. We believe that the spatial heterogeneity of the spongy in the individual model leads to the large RDM. The distribution of spongy is uneven, as many studies have mentioned (Sabanciogullari et al., 2012; Zvyagin & Anushkina, 2018). However, both the compact and spongy layers of the skull were composed of concentric spheres in the ideal sphere model, so the uniform thickness keeps the RDM value small.

For temporally interfering electrical stimulation, we simulated the electric field envelope distribution in each direction in spherical head models and individualized human head models. The electric field envelope distributions of the single-layer skull and layered skull spherical model are very similar, with a high Pearson correlation coefficient, and there was no significant difference by *t*-test except in the *y*-direction. However, in the individualized human head models, the electric field envelope distributions of the single-layer skull and layered skull models were not exactly the same, the Pearson correlation coefficient in the *x*-direction was low, and the *T*-test showed significant differences in each direction. In general, skull stratification in the spherical model had little effect on the temporally interfering electrical stimulation effects, but skull stratification had a significant effect in the individual model. The reason for this result may be the irregular shape of the spongy layer in the skull. An obvious difference between the spongy thickness at various anthropologic points of the skull was observed, and the midfrontal, back and front bregma, lambda, opisthocranium, and euryon points were used in the measurement (Sabanciogullari et al., 2012). According to the measurements carried out at several anthropologic points from the cranial magnetic resonance images, a meaningful statistical linear correlation between age and spongy thickness was determined (Zvyagin & Anushkina, 2018). In view of the universal phenomenon of uneven spongy thickness distribution, the difference in electrical stimulation between individual layered skull and single-layer skull models reflected in the simulation may exist in the actual situation. Consequently, the skull should be divided into compacta and spongy in the simulation of electrical stimulation for accuracy of the kHz tACS stimulation intensity and the target position of temporally interfering electrical stimulation.

The neural modulation frequency of temporally interfering electrical stimulation is based on the frequency of the electric field envelope equal to the difference frequency. As long as the difference frequency is fixed, a similar activation effect can be achieved even though the carrier frequency is different. From the simulation level, we find that an increase in carrier frequency can increase the electric field envelope amplitude without affecting the pattern of electric field envelope

amplitude. However, from the feedback of neurons, it is more difficult for a high carrier frequency to cause nerve firing (Grossman et al., 2017). This is a contradictory problem in the choice of carrier frequency: a higher carrier frequency can generate a stronger electric field envelope amplitude at the same current density, but the unit envelope amplitude induces reduced neural activation. Therefore, it is necessary to combine simulation research and electrophysiological research to find the optimal carrier frequency.

5 | CONCLUSION

This article studied the influence of constructing a three-layer skull model on the stimulation effects in the simulation of tACS and temporally interfering electrical stimulation. In the spherical head model, the layered skull can improve the model sensitivity to the frequency variation of tACS but has no significant effect on the pattern of the electric field. In an individualized human head model, the layered skull model can improve the sensitivity of the model to the frequency and change the pattern of the electric field compared to a single-layer model. Temporally interfering electrical stimulation can be considered the simultaneous action of multiple kHz tACS. Therefore, based on the previous conclusion of tACS and further simulations, we found that an increase in carrier frequency can improve the stimulus intensity, which provides an idea for the selection of carrier frequency. In addition, through the comparison of the electric field envelope amplitude distribution between the single-layer skull model and layered skull model, we found that in the individual model, both the *t*-test and Pearson correlation analysis results showed differences. Ultimately, we concluded that it is necessary to construct a three-layered skull with an accurate spongy shape for electrical stimulation simulation in an individualized model in order to improve the accuracy of the prediction of stimulus intensity and stimulus target.

ACKNOWLEDGMENTS

We thank our research participants and their families for their motivation, adherence, and dedication that made this study possible. This work was supported by the National Key R&D Program of China (grant number 2018YFC0115400), the National Natural Science Foundation of China (grant numbers 61727807, 82071912), the Beijing Municipal Science and Technology Commission (grant numbers Z191100010618004).

CONFLICT OF INTERESTS

The authors declare no conflicts of interest.

DATA AVAILABILITY STATEMENT

Deidentified data that support the findings of this study are available from the corresponding author upon reasonable request.

ORCID

Heng Wang  <https://orcid.org/0000-0002-8368-4502>

Chunlin Li  <https://orcid.org/0000-0002-4437-558X>

Tianyi Yan  <https://orcid.org/0000-0002-2674-4134>

REFERENCES

- Akhtari, M., Bryant, H. C., Mamelak, A. N., Flynn, E. R., Heller, L., Shih, J. J., ... Sutherling, W. W. (2002). Conductivities of three-layer live human skull. *Brain Topography*, *14*, 151–167.
- Ali, M. M., Sellers, K. K., & Frohlich, F. (2013). Transcranial alternating current stimulation modulates large-scale cortical network activity by network resonance. *Journal of Neuroscience*, *33*, 11262–11275.
- Bikson, M., Datta, A., Rahman, A., & Scaturro, J. (2010). Electrode montages for tDCS and weak transcranial electrical stimulation: Role of "return" electrode's position and size. *Clinical Neurophysiology*, *121*, 1976–1978.
- Chen, L., Zou, X., Tang, R., Ke, A., & He, J. (2019). Effect of electrode-electrolyte spatial mismatch on transcranial direct current stimulation: A finite element modeling study. *Journal of Neural Engineering*, *16*, 056012.
- Daa, B., Antonenko, D., Gbasc, D., Ittermann, B., Grüttner, U., & Flöel, A. (2019). Towards precise brain stimulation: Is electric field simulation related to neuromodulation? *Brain Stimulation*, *12*(5), 1159–1168.
- Datta, A., Elwassif, M., Battaglia, F., & Bikson, M. (2008). Transcranial current stimulation focality using disc and ring electrode configurations: FEM analysis. *Journal of Neural Engineering*, *5*, 163–174.
- Elsner, B., Kugler, J., Pohl, M., & Mehrholz, J. (2016). Transcranial direct current stimulation for improving idiopathic Parkinson's syndrome: An abridged version of a cochrane review. *European Journal of Physical and Rehabilitation Medicine*, *52*, 902–906.
- Fregni, F., Boggio, P. S., Santos, M. C., Lima, M., Vieira, A. L., Rigonatti, S. P., ... Pascual-Leone, A. (2006). Noninvasive cortical stimulation with transcranial direct current stimulation in Parkinson's disease. *Movement Disorders*, *21*, 1693–1702.
- Fujimoto, S., Kon, N., Otaka, Y., Yamaguchi, T., Nakayama, T., Kondo, K., ... Tanaka, S. (2016). Transcranial direct current stimulation over the primary and secondary somatosensory cortices transiently improves tactile spatial discrimination in stroke patients. *Frontiers in Neuroscience*, *10*, 128.
- Gabriel, C., Gabriel, S., & Corthout, E. (1996). The dielectric properties of biological tissues: I. literature survey. *Physics in Medicine and Biology*, *41*, 2231–2249.
- Grossman, N., Bono, D., Dedic, N., Kodandaramaiah, S. B., Rudenko, A., Suk, H. J., ... Boyden, E. S. (2017). Noninvasive deep brain stimulation via temporally interfering electric fields. *Cell*, *169*, 1029–1041.e16.
- Hauelsen, J., Ramon, C., Eiselt, M., Brauer, H., & Nowak, H. (1997). Influence of tissue resistivities on neuromagnetic fields and electric potentials studied with a finite element model of the head. *IEEE Transactions on Biomedical Engineering*, *44*, 727–735.
- Holmes, M. D., Feng, R., Wise, M. V., Ma, C., Ramon, C., Wu, J., ... Tucker, D. M. (2019). Safety of slow-pulsed transcranial electrical stimulation in acute spike suppression. *Annals of Clinical and Translational Neurology*, *6*, 2579–2585.
- Homma, S., Musha, T., Nakajima, Y., Okamoto, Y., Blom, S., Flink, R., & Hagbarth, K. E. (1995). Conductivity ratios of the scalp-skull-brain head model in estimating equivalent dipole sources in human brain. *Neuroscience Research*, *22*, 51–55.
- Indahlstari, A., Albizu, A., O'Shea, A., Forbes, M. A., Nissim, N. R., Kraft, J. N., ... Woods, A. J. (2020). Modeling transcranial electrical stimulation in the aging brain. *Brain Stimulation*, *13*, 664–674.
- Kaski, D., Allum, J. H., Bronstein, A. M., & Dominguez, R. O. (2014). Applying anodal tDCS during tango dancing in a patient with Parkinson's disease. *Neuroscience Letters*, *568*, 39–43.
- Kaski, D., Dominguez, R. O., Allum, J. H., Islam, A. F., & Bronstein, A. M. (2014). Combining physical training with transcranial direct current stimulation to improve gait in Parkinson's disease: A pilot randomized controlled study. *Clinical Rehabilitation*, *28*, 1115–1124.
- Laakso, I., Mikkonen, M., Koyama, S., Hirata, A., & Tanaka, S. (2019). Can electric fields explain interindividual variability in transcranial direct current stimulation of the motor cortex? *Scientific Reports*, *9*, 626.
- Mikkonen, M., Laakso, I., Tanaka, S., & Hirata, A. (2020). Cost of focality in TDCS: Interindividual variability in electric fields. *Brain Stimulation*, *13*, 117–124.
- Mutz, J., Edgcombe, D. R., Brunoni, A. R., & Fu, C. H. Y. (2018). Efficacy and acceptability of noninvasive brain stimulation for the treatment of adult unipolar and bipolar depression: A systematic review and meta-analysis of randomised sham controlled trials. *Neuroscience and Biobehavioral Reviews*, *92*, 291e303.
- Nielsen, J. D., Madsen, K. H., Puonti, O., Siebner, H. R., Bauer, C., Madsen, C. G., ... Thielscher, A. (2018). Automatic skull segmentation from MR images for realistic volume conductor models of the head: Assessment of the state-of-the-art. *Neuroimage*, *174*, 587–598.
- Nitsche, M. A., Liebetanz, D., Antal, A., Lang, N., Tergau, F., & Paulus, W. (2003). Modulation of cortical excitability by weak direct current stimulation—technical, safety and functional aspects. *Supplementary of Clinical Neurophysiology*, *56*, 255–276.
- O'Connell, N. E., Marston, L., Spencer, S., DeSouza, L. H., & Wand, B. M. (2018). Non-invasive brain stimulation techniques for chronic pain. *Cochrane Database of Systematic Reviews*, *3*, 14–21.
- Puonti, O., Saturnino, G. B., Madsen, K. H., & Thielscher, A. (2020). Value and limitations of intracranial recordings for validating electric field modeling for transcranial brain stimulation. *Neuroimage*, *208*, 116431.
- Rampersad, S. M., Stegeman, D. F., & Oostendorp, T. F. (2013). Single-layer skull approximations perform well in transcranial direct current stimulation modeling. *IEEE Transactions on Neural Systems and Rehabilitation Engineering*, *21*, 346–353.
- Rashed, E. A., Gomez-Tames, J., & Hirata, A. (2020). End-to-end semantic segmentation of personalized deep brain structures for non-invasive brain stimulation. *Neural Networks*, *125*, 233–244.
- Rush, S., & Driscoll, D. A. (1968). Current distribution in the brain from surface electrodes. *Anesthesia & Analgesia*, *47*, 717–723.
- Sabanciogullari, V., Kosar, M. I., Salk, I., Erdil, F. H., Oztoprak, I., & Cimen, M. (2012). Diploe thickness and cranial dimensions in males and females in mid-Anatolian population: An MRI study. *Forensic Science International*, *219*, 289.e1–289.e7.
- Schulz, R., Gerloff, C., & Hummel, F. C. (2013). Non-invasive brain stimulation in neurological diseases. *Neuropharmacology*, *64*, 579–587.
- Suh, H. S., Lee, W. H., & Kim, T. S. (2012). Influence of anisotropic conductivity in the skull and white matter on transcranial direct current stimulation via an anatomically realistic finite element head model. *Physics in Medicine & Biology*, *57*, 6961–6980.
- Tavakoli, A. V., & Yun, K. (2017). Transcranial alternating current stimulation (tACS) mechanisms and protocols. *Frontiers in Cellular Neuroscience*, *11*, 214.
- Voroslakos, M., Takeuchi, Y., Brnyiczki, K., Zombori, T., Oliva, A., Fernandez-Ruiz, A., ... Berenyi, A. (2018). Direct effects of transcranial electric stimulation on brain circuits in rats and humans. *Nature Communications*, *9*, 483.
- Wang, H., Shi, Z., Sun, W., Zhang, J., Wang, J., Shi, Y., ... Xu, Y. (2020). Development of a non-invasive deep brain stimulator with precise positioning and real-time monitoring of bioimpedance. *Frontiers in Neuroinformatics*, *14*, 574189.
- Wolters, C. H., Anwander, A., Tricoche, X., Weinstein, D., Koch, M. A., & MacLeod, R. S. (2006). Influence of tissue conductivity anisotropy on EEG/MEG field and return current computation in a realistic head model: A simulation and visualization study using high-resolution finite element modeling. *Neuroimage*, *30*, 813–826.
- Zvyagin, V. N., & Anushkina, E. S. (2018). Determining the age of the children from the cranial cranium vault fragments with the use of the modern investigative techniques. *Sudebno Meditsinskaia Ekspertiza*, *61*, 13–16.

How to cite this article: Wang, H., Sun, W., Zhang, J., Yan, Z., Wang, C., Wang, L., Liu, T., Li, C., Chen, D., Shintaro, F., Wu, J., & Yan, T. (2021). Influence of layered skull modeling on the frequency sensitivity and target accuracy in simulations of transcranial current stimulation. *Human Brain Mapping*, *42*(16), 5345–5356. <https://doi.org/10.1002/hbm.25622>